

## Experiments on nonlinear radiation trapping in a saturable atomic vapor

T. Scholz, J. Welzel, and W. Lange

*Institut für Angewandte Physik, Westfälische Wilhelms-Universität Münster, Corrensstraße 2/4, D-48149 Münster, Germany*

(Received 29 April 2001; published 17 September 2001)

We present experiments of a laser with variable pulse energy and beam width saturating sodium vapor near the  $D_1$ -line transition. At high optical depth and in a buffer gas atmosphere of argon, the effect of nonlinear radiation trapping is shown to drastically change the spatial distribution and temporal evolution of the excited-state population and of the fluorescence light trapped by the nonlinear medium. Besides observing the transient behavior of the fluorescence light, a pump-probe beam experiment enables us to gain a tomographic view inside the atomic vapor. Nitrogen as a buffer gas is used to compare with the situation where radiation trapping effects are negligible. Finally, numerical simulations based upon equations of radiative transfer for a two-level atomic system elucidate the role of nonlinear radiation trapping and support given interpretations of the experiments.

DOI: 10.1103/PhysRevA.64.043409

PACS number(s): 32.80.-t, 32.70.Jz

### I. INTRODUCTION

In an optically thick atomic vapor excited by a laser beam, the process of multiple scattering of fluorescence light—also called radiation trapping or radiation diffusion—is a long known effect [1,2] that significantly alters the temporal and spatial behavior of the population of the excited state. Radiation trapping plays an important role, e.g., in plasma physics and, chemical physics, astrophysics and has been studied in great detail both theoretically (cf., e.g., [1–11]) and experimentally (cf., e.g., [12–16]). It is obvious that this process also exists in many experiments dealing with nonlinear optics where an intense laser beam interacts with an atomic sample of large optical depth [8,17,18]. However, the description of radiation trapping is very complex so it is often neglected in the analysis of nonlinear optical experiments.

In the situation of a strong laser beam saturation must be taken into account, additionally. Saturation of an atomic transition gives rise to a pronounced nonlinear behavior of the scattered fluorescence light. This effect of nonlinear radiation trapping results in unexpected phenomena: An atomic sample saturated over the whole cross section by a laser pulse emits fluorescence light decaying *subnaturally* [19,20] in contrast to the well-known prolonged decay times caused by linear radiation trapping [2]. This counterintuitive behavior can be explained by the spatially and temporally interlocked evolution of the population of the excited state being the origin of the process of nonlinear radiation trapping.

In this paper, a related experiment to the one mentioned above is described. The behavior of the subnatural decay is not only investigated in more detail, the spatial and temporal behavior of the population of the excited state and its dependence on the pump pulse characteristics is determined, simultaneously, to elucidate the complex interplay of saturation and radiation trapping. In contrast to the experiment presented in Ref. [20] a—in relation to the extended atomic sample—narrow Gaussian laser beam is used. This is more typical for experiments involving laser interaction processes.

Fluorescence light escaping the cell geometry is measured at the border of the sample, so there is no directly excited

sodium vapor between the laser beam and the detector. On the other hand, the spatial and temporal dependence of the population of the excited state is determined by a second continuous laser beam propagating antiparallel to the pump laser pulse. While the observation of the radiation leaving the sample gives just a global quantity depending in a complicated way on the processes within the atomic vapor, the probe beam technique allows a tomographic view inside the medium. Determining the population of the excited state, a much more direct comparison between experiment and theory should be feasible. With the help of a quenching buffer gas, we are able to compare the situation with the one where radiation trapping effects are negligible.

### II. EXPERIMENTAL SETUP AND PARAMETERS

The experimental setup is illustrated in Fig. 1(a). Sodium vapor is contained in a cylindrical glass cell of 2 cm diameter and 3 cm length of the heated zone. The sodium resistant glass cell can be heated up to 420 °C. The particle density at a measured temperature of the cell is determined with the help of the linear Faraday effect at low argon pressure ( $\leq 2$  hPa) [21]. At temperatures of the sodium cell of 200,

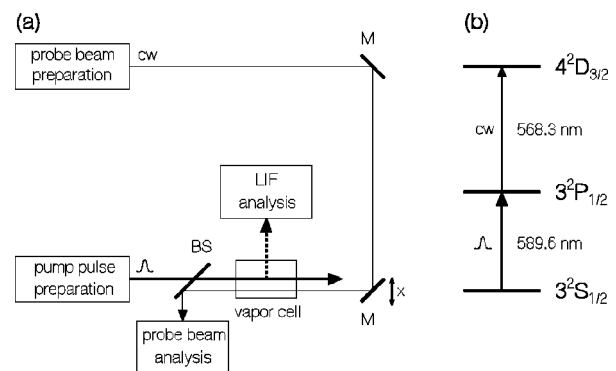


FIG. 1. (a) Schematic of the experimental setup. BS, beam splitter; cw, continuous wave; LIF, laser induced fluorescence; M, mirror; (b) sodium level scheme for the pump-probe beam experiment with stepwise excitation.

240, and 280 °C, used for the experiments in this paper, the measured particle density amounts to  $(2.1 \pm 0.3) \times 10^{12}$ ,  $(1.6 \pm 0.2) \times 10^{13}$ , and  $(7.5 \pm 1.1) \times 10^{13} \text{ cm}^{-3}$ . Further measurements are carried out in an atmosphere of 20 hPa argon (Ar) or 20 hPa nitrogen ( $N_2$ ), respectively. The corresponding optical depths  $k_0 R$ , defined by the product of the unsaturated absorption coefficient  $k_0$  on line center and the characteristic length  $R = 1 \text{ cm}$  of the cell geometry, are of about 8, 60, and 280.

The pump pulse preparation [cf. Fig. 1(a)] is performed with a Q-switched and frequency doubled Nd:YAG-laser (Spectra-Physics, Model No. DCR-3), which pumps a tunable dye laser in a grazing incidence arrangement (cf. [22]). The pump laser employs injection seeding that results in a very smooth pulse shape. This proves to be favorable with respect to the bandwidth of the dye laser. A spectral width of  $240 \pm 60 \text{ MHz}$  is determined, hence, though with exception of the grating, no elements reducing the line width are used, the dye laser pulse is nearly Fourier limited.

The laser pulse is spatially filtered and injected on the axis of the vapor cell. It is tuned into the vicinity of the  $D_1$ -line transition  $3^2S_{1/2} \rightarrow 3^2P_{1/2}$  [Fig. 1(b)] of the sodium vapor. The intensity distribution  $I_p$  of the laser pulse is nearly Gaussian in time and space

$$I_p(r, t) = I_{max} \exp\left(-2 \frac{r^2}{w_p^2}\right) \exp\left(-2 \frac{t^2}{\tau_p^2}\right). \quad (1)$$

The beam radius  $w_p$  of the pump pulse is varied with the help of an optical spatial filter (telescope) from  $1.8 \pm 0.1$  to  $3.6 \pm 0.2 \text{ mm}$ . The maximum energy per pulse is about 300  $\mu\text{J}$  with a pulse duration of  $\tau_p = 7.0 \pm 0.5 \text{ ns}$ . However, the intensity of the pump pulse is strong enough to saturate the medium justifying to neglect pump-wave depletion. With respect to the collimated and resonant pump laser, self refraction can be dropped as well.

For reference purposes, the transients of the fluorescence light escaping the glass cell in a direction perpendicular to the exciting laser beam are detected by a photomultiplier and analyzed by means of a fast digital oscilloscope with a maximum sampling rate of 2 GS/s single shot (LeCroy, Model No. 9354 L).

For a spatially resolved probing of the time-dependent population of the  $3^2P_{1/2}$  state over the cross section of the atomic sample, a probe beam from a cw ring dye laser is used tuned near the  $3^2P_{1/2} \rightarrow 4^2D_{3/2}$  transition [Fig. 1(b)]. Operation is ensured in the regime characterized by a linear dependence of the absorption on the population of the excited state by detuning the probe laser slightly with respect to the probe transition. The population of the excited state can be determined at every point in the cylindrical cell by this tomographic method. Antiparallel beam propagation of the pump and probe beam is preferred for the measurements. With the help of a micromanipulator and a mirror [cf. Fig. 1(a)] the probe beam (radius:  $w_{cw} \approx 0.2 \text{ mm} \ll w_p$ ) can be displaced with respect to the pump beam to obtain the radial dependence of the population of the excited state. The temporal evolution of the probe beam absorption is measured

with the help of a detector and the digital oscilloscope. An interference filter only transmits the probe beam in order to separate it from fluorescence and light scattered from the pump beam. Furthermore, it is ensured that the whole transmitted light from the probe beam is detected with the help of a photomultiplier having a relatively large sensitive area coupled with a fast response. Also, any further apertures in the beam trace are avoided, hence, small refraction or diffraction that the probe beam may experience does not have any significant influence on the results.

### III. EXPERIMENTAL RESULTS

Normalized values of the temporal evolution of the population of the excited state—designated with  $s$ —in the middle of the cell and of the intensity of the fluorescence escaping the cell are shown in Figs. 2(a) and 2(b) for two different pump pulse energies, respectively. Both signals decay monotonically after a very fast increase when the laser pulse appears. Closer inspection of the time behavior reveals for large times after the pulse, a nearly exponential decay that corresponds to the decay of the slowest mode occurring in the well known Holstein theory of radiation trapping [2,3]. In the time immediately after the pulse, the decay is much faster and shows a pronounced dependence on the input energy of the pump pulse. By considering the slope of the curve, we can determine a *momentary decay constant* that is fastest in the period 10 ns after the maximum of the pump pulse occurs, illustrated in an expanded view in Figs. 2(c) and 2(d) with logarithmic ordinate. The decay constants of the fluorescence light are 41.0 ns for small pulse energy and 11.2 ns

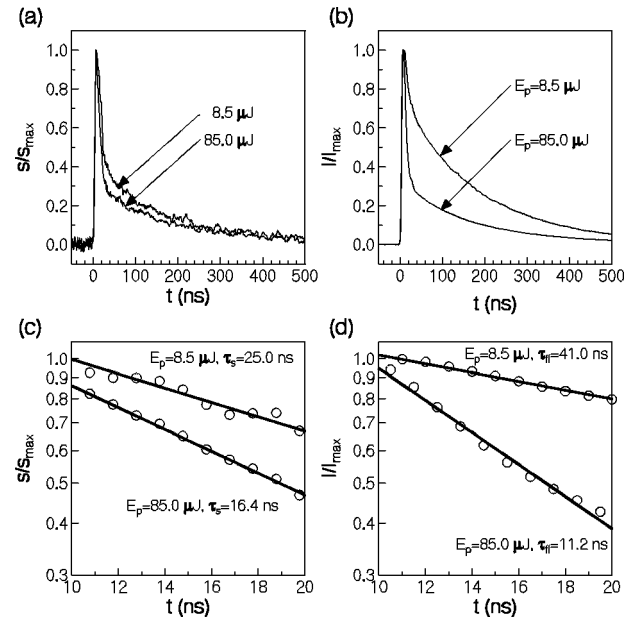


FIG. 2. Dependence on the input energy of the pump pulse. (a) Normalized transients of the on axis population of the excited  $3^2P_{1/2}$  state; (b) normalized transients of the fluorescence intensity escaping the vapor cell. (c), (d) Logarithmic representation of the same properties such as those in (a), (b) at times 10 to 20 ns after the pump pulse has disappeared.  $w_p = 3.6 \text{ mm}$ ;  $\tau_p = 7 \text{ ns}$ ;  $p = 20 \text{ hPa Ar}$ ;  $T = 240 \text{ }^\circ\text{C}$ .

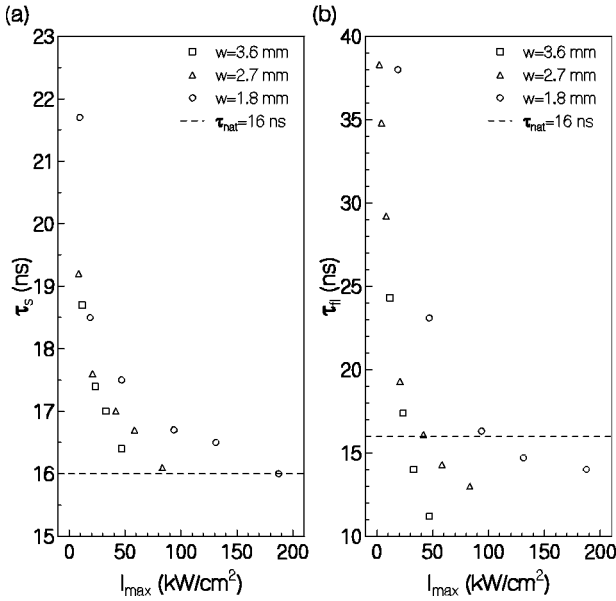


FIG. 3.  $1/e$ -decay times of the population of the  $3^2P_{1/2}$  state at  $x=0$  mm (a) and the total fluorescence intensity (b) fitted to the experimental data 10–30 ns after the pulse has reached its maximum intensity.  $\tau_p=7$  ns;  $p=20$  hPa Ar;  $T=240$  °C. Standard deviations,  $I_{max}$ ;  $\tau_{fl}$ ,  $\pm 10\%$ ;  $\tau_s$ ,  $\pm 15\%$ .

for higher pulse energy, the last being less than the natural decay time of 16 ns, even considering a time resolution of about 2 ns. The corresponding results for the population of the excited state are 25.0 and 16.4 ns. This is not faster than the natural decay time of the  $D_1$ -line transition.

An explanation of this counterintuitive effect can be given as follows: The optical depth of the atomic sample is reduced effectively by saturation in the region of the directly excited volume. Additionally, multiple scattered fluorescence photons increase the intensity flux that is present inside the whole medium. In the case of high optical depth, the trapping process is concentrated in the vicinity of the laser beam [14] due to an increase in reabsorption probability. A continuously growing saturation region decreases the effective optical depth. After the decay of the saturation, a certain time after the pump pulse has disappeared, the optical depth increases rapidly causing a sudden breakdown of the photon flux to the detector. All of these interlocked spatial and temporal effects result in a subnatural decay. The larger the saturated region is, the faster the subnatural decay will be, what indeed is observed.

Figure 3 represents the fastest effective decay times in dependence of the pump pulse intensity for different beam radii for the on-axis population of the excited state and for the fluorescence light. Given a beam radius of 1.8 mm, the subnatural decay is first observed at an intensity of about 90 kW/cm<sup>2</sup>. For a beam radius of 3.6 mm, only less than the half of the pump pulse intensity is needed. On the other hand, the corresponding effective decay times of the population of the excited state do not fall under the natural limit.

In the vicinity of the direct excited volume there is established a substantial amount of population of the excited state due to radiation trapping. Figure 4 represents the temporal

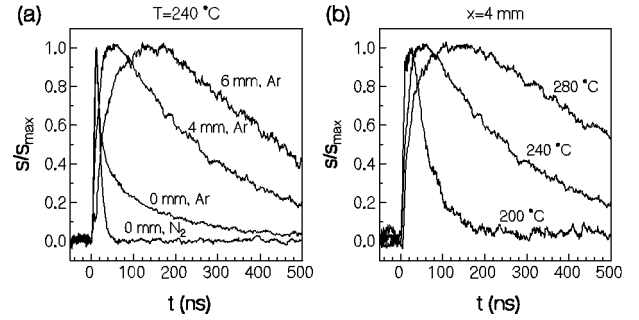


FIG. 4. (a) Normalized transient behavior of the population of the  $3^2P_{1/2}$  state given by the absorption of the cw probe-laser beam for different displacements  $x$  of the probe beam from the axis of the pump beam.  $s_{max}(x=4$  mm) $=0.22\pm 0.03$  and  $s_{max}(x=6$  mm) $=0.10\pm 0.02$ , if  $s$  is assumed to saturate ( $s=0.5$ ) at  $x=0$  mm. (b) Normalized transient behavior of the population of the  $3^2P_{1/2}$  state 4 mm outside the axis of the pump beam for different temperatures (optical depths) of the vapor cell. Further parameters: pump beam radius,  $w_p=1.8$  mm; probe-beam radius,  $w_{cw}=0.2$  mm; pulse duration,  $\tau_p=7$  ns; energy per pulse,  $E_p=85$   $\mu$ J; buffer gas pressure,  $p=20$  hPa Ar/N<sub>2</sub>.

behavior of the normalized population of the excited state. Figure 4(a) compares the behavior at different transverse positions of the probe beam at a cell temperature of 240 °C. Figure 4(b) shows the same situation at a distinct spatial position and different temperatures of the heated cell. In the center of the cell, the population of the excited state decreases monotonically after the pump pulse has disappeared. Its maximum retards for finite delay off axis. The delay is increasing with distance from the axis. Furthermore, the delay grows at higher optical depth, because more reabsorption processes are necessary to transfer excitation outside the pump beam volume after saturation is decaying. These results are intuitively expected from the linear radiation trapping theory [2]. The experimental data relating to Fig. 4 uncover the relation between the maximum population of the excited state for different displacements with the assumption of complete saturation of 100% on axis: At 4 mm displacement  $44\pm 3\%$  and at 6 mm  $20\pm 2\%$  are reached.

For a comparison with the situation where the influence of radiation trapping is negligible, nitrogen is used instead of argon as a buffer gas. Nitrogen is known to quench the excited state population very effectively. The strength of the impact broadening is within a few percent the same as for the broadening of argon. At a buffer gas pressure of 20 hPa, the quench rate equals the natural decay rate of the sodium  $D_1$ -line transition [23]. The population of the excited state decays twice as fast in the case of nitrogen as in the case of argon. This result is also manifested in Fig. 4(a): The population of the excited state on axis decays rapidly after the pump pulse has vanished. Off axis, no absorption signal is measured at all. In the case of a quenching buffer gas, the population of the excited state is concentrated on the pump beam volume only. In conclusion, nitrogen as a buffer gas offers the possibility to reduce or nearly cancel effects due to radiation trapping.

The delay of the maximum population of the excited state with respect to the maximum of the pump pulse intensity [cf.

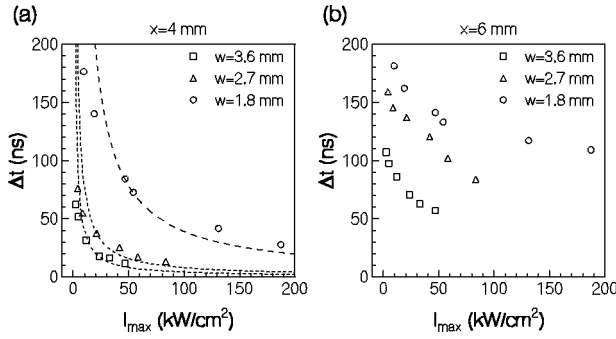


FIG. 5. Rise time for the maximum population of the  $3^2P_{1/2}$  state for different pulse energies and radii of the pump laser beam at  $x=4$  mm (a) and  $x=6$  mm (b) displacement of the probe from the pump laser beam (cf. Fig. 1). Dashed line,  $\Delta t \sim 1/I_{max}$  fitted to the experimental data.  $\tau_p = 7$  ns;  $p = 20$  hPa Ar;  $T = 240$  °C. Standard deviations,  $I_{max}$ ;  $\Delta t$ ,  $\pm 10\%$ .

Eq. (1)] strongly depends upon the pump pulse energy. In Fig. 5 this dependence is shown for different beam diameters and two distances off axis. The temporal dependence is in qualitative agreement with the theoretical predictions given in Ref. [9], where the temporal evolution of the population of the excited state is calculated in different geometries with the approximation of an inner saturated volume and an outer region which is not directly excited. But there, neither the spatial characteristics nor the temporal evolution of the laser pulse are taken into account. As a consequence, no dependence of the atomic variables on the external pump occurs. A similar ansatz was made in Ref. [19] where the subnatural decay was predicted theoretically. To elucidate the role of nonlinear radiation trapping, a theoretical and numerical analysis of the experimental situation is given in the following two chapters.

#### IV. THEORY

For a theoretical description of the radiation trapping process, the equation of radiative transfer is solved (cf. [24]) in combination with a rate equation for the population of the excited state. By formal integration, the Holstein equation of radiation trapping can be derived. We apply the two-level approximation for the atomic line here, neglecting fine and hyperfine structure.

At a buffer gas pressure of 20 hPa Ar or  $N_2$ , used in the experiments, the transverse relaxation rates due to Na-Ar or Na- $N_2$  collisions equal  $\Gamma_2 \approx 780$  MHz [25]. Hence, the absorbed and emitted light can be considered as nearly uncorrelated in frequency [ $\Gamma_2/(\Gamma_2 + \Gamma_1) \approx 0.93$ ; cf. [26]] and complete frequency redistribution can be employed.

The spectral absorption coefficient  $k$  is assumed not to depend on the pump pulse evolution. Rabi splitting [27] in the case of resonant excitation by the laser pulse is omitted, because the maximum Rabi frequency is significantly less than the broadening of the atomic resonance line. Another approximation is, that the influence of the flight time of photons and of the particle diffusion of atoms can be neglected compared to the lifetime of the population of the excited state. The first assumptions holds for the spatial dimensions

of a small vapor cell, not, e.g., for extended or natural systems as in astrophysics.

Due to the cylindrical geometry of the problem, limitations in computer memory and CPU time, the discussion is restricted to one spatial dimension. We derive two simplified equations for the normalized spectral fluorescence light intensity  $\tilde{J}_{\pm} = J_{\pm}/J_{sat}$  traveling in the positive and negative  $x$  direction, respectively:

$$\pm \frac{\partial}{\partial x} \tilde{J}_{\pm}(x, t, \nu) = \frac{1}{2} k(\nu) s(x, t) - k(\nu) \{1 - 2s(x, t)\} \tilde{J}_{\pm}(x, t, \nu). \quad (2)$$

$x \in [-R, +R]$  is the coordinate transverse the laser beam (cf. Fig. 1).  $R$  represents the radius of the cell containing the sodium vapor,  $t$  is the time, and  $\nu$  the frequency of the fluorescence light.  $J_{sat} = 8\pi hc/\lambda^3$  defines the spectral saturation intensity (2.4 W/[cm<sup>2</sup> GHz] for the sodium  $D_1$  line).  $k = \kappa\phi$  describes the spectral absorption coefficient with the normalized Voigt function  $\phi = \phi(\nu)$  ( $\int_{-\infty}^{+\infty} d\nu \phi(\nu) = 1$ ; cf. [28]) and  $\kappa = \lambda^2 N \Gamma_1 / (8\pi)$ .  $\lambda$  represents the wavelength of the  $D_1$ -line transition and  $N$  is the measured particle density of sodium atoms.  $s$  defines the population of the excited atomic state in space and time normalized onto the total number of atoms. The term  $\{1 - 2s(x, t)\}$  accounts for stimulated emission processes under the assumption of particle conservation.

The temporal evolution of the population of the excited state  $s$  can be determined with the help of a rate equation

$$\frac{\partial}{\partial t} s(x, t) = P(x, t) \{1 - 2s(x, t)\} - (\Gamma_1 + Q) s(x, t). \quad (3)$$

$\Gamma_1 = 1/\tau_{nat}$  represents the longitudinal relaxation rate and  $\tau_{nat}$  is the lifetime of the excited state.  $Q$  describes the rate due to quenching collisions of sodium atoms in the excited state with  $N_2$  molecules [23,29]. Quenching due to Na- $Na_2$  collision can be neglected [14].  $Q \approx 56$  MHz at a pressure of 20 hPa  $N_2$  and a cell temperature of 240 °C.

$P(x, t)$  equals the net pump rate at a given distance off axis and time consisting of two components

$$P = P_{ex} + P_{fl}, \quad (4)$$

$$P_{ex} = \Omega_R^2(x, t) \phi(\nu_{Laser}), \quad (5)$$

$$P_{fl} = \Gamma_1 \int_{-\infty}^{+\infty} d\nu \phi(\nu) \{ \tilde{J}_+(x, t, \nu) + \tilde{J}_-(x, t, \nu) \}. \quad (6)$$

$P_{ex}(x, t) \sim I_p(x, t)$  [cf. Eq. (1)] is the pump rate of the Gaussian laser pulse and  $\Omega_R(x, t) = \mu \tilde{\mathcal{E}}(x, t) / (2\hbar)$  is the Rabi frequency. Here,  $\mu$  represents the dipole matrix element of the  $D_1$ -line transition,  $\hbar$  is Planck's constant, and  $\tilde{\mathcal{E}}$  describes the envelope of the laser field.

In contrast to [9,20], the transient behavior of the short external pump pulse is included in the theoretical treatment.  $P_{ex}$  describes the pump rate of the external pump pulse of the laser and  $P_{fl}$  is the pump rate due to the internally

trapped fluorescence calculated with the help of Eq. (2). The basic system of differential equations for the light on the one hand and for the properties of the atomic medium on the other hand are coupled via  $P_{fl}$ . The resulting terms  $s\tilde{J}_{\pm}$  in Eq. (3) represent the internal nonlinearity induced by the multiple scattering of intense fluorescence light.

In the case of a fully saturated medium ( $s \equiv 1/2$ ), the effective spectral absorption coefficient  $k_{eff} = k(1 - 2s)$  and all radiation trapping processes vanish [cf. Eqs. (2) and (3)]. Hence, the population and the fluorescence decay with the natural lifetime  $\tau_{nat} = 1/\Gamma_1$ , if no quenching collisions occur. After applying a short intense laser pulse, the saturation decreases and nonlinear radiation trapping sets in.

## V. NUMERICAL CALCULATION AND DISCUSSION

Equations (2) and (3) are evaluated on a grid in real space (cf. e.g. Ref. [30]) and real frequency space. They are integrated for more than  $10^3$  spatial positions and real frequencies and  $10^6$  time steps. The initial condition is given by  $s(x, t_0) = 0$  for  $x \in [-R, +R]$  with open boundary conditions (no reflecting walls).  $t_0$  is chosen to satisfy  $P(x, t_0)$  to be negligible. Due to the computational restrictions discussed, we cannot compare calculations to all our experimental results.

First, Fig. 6 shows the calculated spatial distribution and temporal evolution of the population of the  $3^2P_{1/2}$  state of sodium vapor for different positions  $x$  [Fig. 6(a)] and different optical depth  $k_0R$  [Fig. 6(b)]. The calculated curves are in good agreement with the behavior observed experimentally (cf. Fig. 4). At  $x = 4$  mm outside the pump beam ( $w_p = 1.8$  mm) and  $T = 240$  °C ( $k_0R = 60$ ), the maximum of the population of the excited state 50 ns after the occurrence of the pump pulse amounts to 24.5% in the calculation. However, this is one half of the saturation value  $s = 1/2$ , indicating the high intensity of the trapped fluorescence to strongly populate the excited state of the atomic vapor outside the pump beam volume. Without inclusion of radiation trapping,

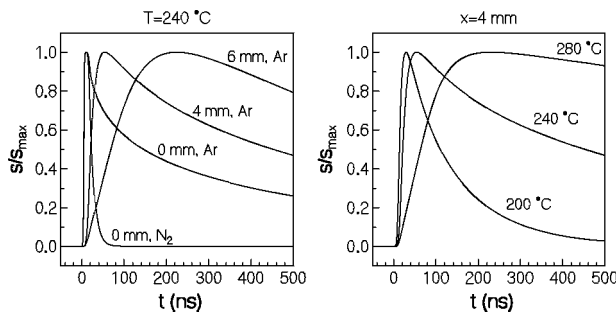


FIG. 6. Calculated transients [cf. Eqs. (2),(3)] of the normalized population of the excited state for different transverse positions  $x$  from the pump beam axis (a) and for different temperatures (optical depths) of the sodium vapor at  $x = 4$  mm (cf. Fig. 2).  $p = 20$  hPa Ar/N<sub>2</sub>;  $Q = 0/56$  MHz;  $P(x, t) = P_0 \exp(-2x^2/w_p^2) \exp(-2t^2/\tau_p^2)$ ;  $P_0 = 5.0$  GHz  $\gg \Gamma_1$ ;  $\Omega_R = 0.49$  GHz;  $w_p = 1.8$  mm;  $\tau_p = 7$  ns. In the case of Ar as buffer gas in (a):  $s_{max}(x = 0 \text{ mm}) = 0.5$ ;  $s_{max}(x = 4 \text{ mm}) = 0.245$ ,  $s_{max}(x = 6 \text{ mm}) = 0.119$ .

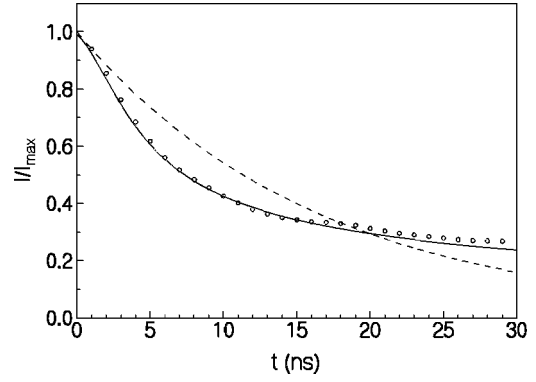


FIG. 7. Open circles, measured subnatural decay of the fluorescence intensity.  $w_p = 3.6$  mm;  $\tau_p = 7$  ns;  $E_p = 85$   $\mu$ J;  $p = 20$  hPa Ar;  $T = 240$  °C. Solid line, calculated behavior of the fluorescence for the experimental parameters. Dashed line, natural decay  $\exp(-t/\tau_{nat})$ .

the population  $s$  of the excited state will not exceed more than a few percent due to the influence of the external pump.

Figure 7 represents the numerical result obtained for the calculation of the transient behavior of the fluorescence light escaping the atomic vapor (solid line), which is also in good agreement with the experimental data (open circles). The fluorescence is shown to decay faster than with the natural lifetime of the atomic level involved (dashed line in Fig. 7).

Finally, Fig. 8 describes the spectral and temporal evolution of the calculated intensity  $J_+ / J_S$  escaping the atomic sample at  $x = R$ . In this representation, the exciting laser pulse reaches its maximum intensity at  $t = 0$ . At this time, the self reversal of the emitted fluorescence light vanishes (*avoided self reversal*), because the intensity of the multiple scattered light outside the laser beam volume is greater than the saturation intensity of the atomic transition ( $J_+ \gg J_S$ ). One concludes, that the rise times in Fig. 5(a) can be approximated by  $\Delta t \sim 1/I$ , if one assumes  $\Delta t \sim k_0R$  (leading

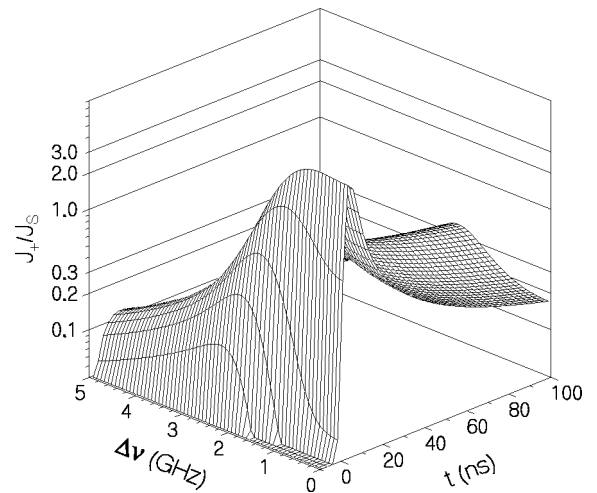


FIG. 8. Calculated spectral intensity  $J_+ / J_S$  at  $x = R$  leaving the atomic vapor in the positive  $x$  direction in dependence of time  $t$  and detuning  $\Delta\nu = \nu - \nu_0$  with respect to the atomic resonance frequency  $\nu_0$ . The parameters are the same as in Fig. 7. The maximum spectral intensity of the multiple scattered light equals  $J_+ = 7.75J_S$ . At  $t = 0$ , the self-reversal of the line shape disappears.

term of  $1/g$  with the escape factor  $g$  for a Doppler broadened line and a cylindrical cell geometry; cf. [12]) and substitutes  $k_0$  by  $k_0/(1+I/I_S)$ , the absorption coefficient of a saturable medium.

In our experiments, the atomic vapor is not only saturated by the spatially limited laser beam inside the pump beam volume, rather it is saturated by the trapped fluorescence light outside this region.

## VI. SUMMARY AND CONCLUSION

In this paper, we introduced a probe beam technique as a tomographical method to study radiation trapping effects. This method determines the spatiotemporal behavior of the population of the excited state, and thus, gives much more direct access to the physical quantities of a *hot* atomic vapor than only the observation of the fluorescence escaping the cell geometry.

A considerable amount of the population of the excited state can be found in a region outside the pump beam volume, produced by resonance fluorescence *diffusing* from the excitation region into the region not directly illuminated. It has to be concluded that the intensity of the trapped fluorescence has to be in the order of magnitude of the saturation intensity of the atomic transition. This additional component of the radiation field, however, significantly increases the ex-

ension of the saturated volume and acts as a nonlocal non-linearity.

It is necessary to include nonlinear radiation trapping effects in a careful analysis of related experiments, especially when examining beam propagation effects in saturable media, four-wave mixing in optically thick vapors, or experiments related to Bose-Einstein condensation [31–33] in *cold* vapors. By observing the time dependence of the fluorescence light in the situation of a narrow laser beam traversing an extended atomic medium, a *subnatural decay* can be well observed. Simultaneous measurements of the population of the excited state never show a decay faster than the natural one. This proves the subnatural decay to be indeed a phenomenon due to nonlinear radiation trapping.

The interpretations of the experimental results are supported by numerical simulations based upon nonlinear equations of radiative transfer. Due to computational limitations numerics is carried out only in one spatial dimension, the coordinate transverse the laser beams. Nevertheless, the experimental results are reproduced quite well, indicating nonlinear radiation trapping to be the decisive effect in our experiments. Furthermore, the numerical results give information about the spectral distribution of the multiple scattered light and the effect of *avoided self reversal* at times where the atomic vapor is strongly saturated due to nonlinear radiation trapping.

- 
- [1] L.M. Biberman, Zh. Éksp. Teor. Fiz. **17**, 416 (1947) [Sov. Phys. JETP **19**, 584 (1949)].
  - [2] T. Holstein, Phys. Rev. **72**, 1212 (1947).
  - [3] T. Holstein, Phys. Rev. **83**, 1159 (1951).
  - [4] C. van Trigt, Phys. Rev. A **13**, 726 (1976).
  - [5] A.W. McCord, R.J. Ballagh, and J. Cooper, Opt. Commun. **68**, 375 (1988).
  - [6] N.J. Mulgan and R.J. Ballagh, Phys. Rev. A **48**, 3321 (1993).
  - [7] X. Ma and R. Lai, Phys. Rev. A **49**, 787 (1994).
  - [8] W. Chalupczak, W. Gawlik, and J. Zachorowski, Phys. Rev. A **49**, R2227 (1994).
  - [9] N.N. Bezuglov, A.N. Klucharev, A.F. Molisch, M. Allegrini, F. Fuso, and T. Staciewicz, Phys. Rev. E **55**, 3333 (1997).
  - [10] N.N. Bezuglov, A.F. Molisch, A.N. Klucharev, F. Fuso, and M. Allegrini, Phys. Rev. A **57**, 2612 (1998).
  - [11] N.N. Bezuglov, A.F. Molisch, A.N. Klucharev, F. Fuso, and M. Allegrini, Phys. Rev. A **59**, 4340 (1999).
  - [12] J. Huennekens and A. Gallagher, Phys. Rev. A **28**, 238 (1983).
  - [13] G. Ankerhold, M. Schiffer, D. Mutschall, T. Scholz, and W. Lange, Phys. Rev. A **48**, 4031 (1993).
  - [14] T. Scholz, M. Schiffer, J. Welzel, D. Cysarz, and W. Lange, Phys. Rev. A **53**, 2169 (1996).
  - [15] S. Basrotti, F. Fuso, A.F. Molisch, and M. Allegrini, Phys. Rev. A **57**, 1778 (1998).
  - [16] N. Sewraj, J.P. Gardou, Y. Salamero, and P. Millet, Phys. Rev. A **62**, 052721 (2000).
  - [17] M. Möller and W. Lange, Phys. Rev. A **49**, 4161 (1994).
  - [18] T. Ackemann, T. Scholz, C. Vorgerd, J. Nalik, L.M. Hoffer, and G.L. Lippi, Opt. Commun. **147**, 411 (1998).
  - [19] T. Staciewicz, T. Kotowski, P. Wiewior, and J. Chorazy, Opt. Commun. **100**, 99 (1993).
  - [20] J. Chorazy, T. Kotowski, and T. Staciewicz, Opt. Commun. **125**, 65 (1996).
  - [21] B.M. Schmidt, J.M. Williams, and D. Williams, J. Opt. Soc. Am. **54**, 454 (1964).
  - [22] M.G. Littmann, Appl. Opt. **23**, 4456 (1984).
  - [23] I. Tanarro *et al.*, J. Chem. Phys. **77**, 1826 (1982).
  - [24] A. Streater, J. Cooper, and W. Sandle, J. Quant. Spectrosc. Radiat. Transf. **37**, 151 (1987).
  - [25] M.J. Jongerius, A.R.D. Van Bergen, T. Hollander, and C.T.J. Alkemade, J. Quant. Spectrosc. Radiat. Transf. **25**, 1 (1981).
  - [26] M.G. Payne, J.E. Talmage, G.S. Hurst, and E.B. Wagner, Phys. Rev. A **9**, 1050 (1974).
  - [27] B.R. Mollow, Phys. Rev. A **5**, 1522 (1972).
  - [28] Z. Shippony and W.G. Read, J. Quant. Spectrosc. Radiat. Transf. **50**, 635 (1993).
  - [29] J. Campos-Martinez, O. Roncero, S. Miret-Artés, P. Villarreal, and G. Delgado-Barrio, J. Chem. Phys. **91**, 155 (1989).
  - [30] G.J. Parker, W.N. Hitchon and J.E. Lawler, J. Phys. B **26**, 4643 (1993).
  - [31] D.W. Sesko, T.G. Walker, and C.E. Wieman, J. Opt. Soc. Am. B **8**, 946 (1991).
  - [32] S. Bali, D. Hoffmann, J. Simán, and T. Walker, Phys. Rev. A **53**, 3469 (1996).
  - [33] L. Pruvost, I. Serre, H.T. Duong, and J. Jortner, Phys. Rev. A **61**, 053408 (2000).